Available online at www.sciencedirect.com

SciVerse ScienceDirect

Ceramics International 38 (2012) 2363–2368

CERAMICS INTERNATIONAL

www.elsevier.com/locate/ceramint

Effect of MgO in the microstructure formation of zirconia mullite composites from sillimanite and zircon

Sasmita Prusty [a], D.K. Mishra [b,*], B.K. Mohapatra [c], S.K. Singh [b]

[a] Geological Survey of India, Alandi Road, Pune 411006, Maharashtra, India

[b] Advanced Materials Technology Department, Institute of Minerals and Materials Technology (CSIR), Bhubaneswar 751013, Odisha, India

[c] Mineralogy Department, Institute of Minerals and Materials Technology (CSIR), Bhubaneswar 751013, Odisha, India

Received 16 June 2011; received in revised form 29 September 2011; accepted 31 October 2011
Available online 6 November 2011

Abstract

The effect of MgO additive on the structural, microstructural and hardness properties of zirconia mullite (MUZ) has been discussed. The MgO additive in MUZ not only stabilizes the cubic zirconia phase but also acts as a sintering aid for the formation of cross-linked mullite grains. The electron micrographs of plasma fused MgO–MUZ shows a uniform arrangement of platelet structure of mullite and dendrite structure of zirconia on mullite surface. The micrograph of plasma sintered composites shows a ladder like structure and a complete cross-linked mullite grains whereas the surface morphology of conventionally sintered composites clearly indicates the presence of small and big grains close packed to each other. Appreciable hardness and higher optical band gap have been observed for plasma fused MgO–MUZ composites. A complete dissociation of sillimanite and zircon has been occurred in plasma fused composites for the complete conversion of MUZ whereas the complete dissociation of sillimanite and zircon has not observed in plasma sintered and conventionally sintered composites. These observations have been realized from the X-ray diffraction and Fourier transform infrared studies.

Keywords: A. Sintering; B. Composites; C. Hardness; D. MgO; D. Mullite

1. Introduction

A lot of research work has been carried out on zirconia–mullite (MUZ) by various groups of researchers due to its super thermo-mechanical properties adopting various synthesis routes and using various kinds of raw materials [1–7]. This material has a lot of importance in ceramic and glass industry due to its high temperature sustainability. The necessity of zirconia additives in the mullite matrix is due to its desirable physical properties such as extremely high melting temperature, high strength and fracture toughness [1,5–7]. When it is used as an additive with mullite, the mechanical and optical properties of mullite are enhanced significantly. Among the three types of polymorphs of zirconia, cubic zirconia is a useful refractory and technical ceramic material because it does not go through destructive phase transitions during heating and cooling. Pure zirconia has no practical importance in the field of ceramic industry or technology to be used as a component due to its limitation of thermal conductivity and due to a large volume change associated with the tetragonal to monoclinic phase transformation on cooling. The cubic form of stabilized zirconia ceramics are of technological importance due to their high oxygen diffusion coefficient, low electronic conductivity, excellent chemical stability under reducing and oxidizing atmospheres at high temperature which are an essential physical parameter needed for a refractory materials [8,9]. Significant materials properties like hardness, toughness, etc. in mullite can be enhanced by introducing tetragonal phase of zirconia mainly by the transformation toughening effect and the formation of microcracks [10–12]. Though it is difficult to achieve a stable cubic phase of zirconia at room temperature, still there are two ways to achieve the cubic phase of zirconia. One is that transform the monoclinic/tetragonal zirconia to cubic zirconia at high temperature and cool the system rapidly, so that cubic zirconia will not get enough time to regain its low temperature monoclinic zirconia phase. The second way is to stabilize the cubic zirconia phase by using additives like Y_2O_3, CaO, MgO, CeO, etc. [2,13–16]. However, the MgO additive

* Corresponding author. Tel.: +91 674 2379456; fax: +91 674 2581637.
E-mail address: dilipiuac@gmail.com (D.K. Mishra).

0272-8842/$36.00
doi:10.1016/j.ceramint.2011.10.089

not only stabilize the cubic zirconia phase but also act as a sintering aid for the formation of cross-linked mullite grains and inter-granular glassy phase [13,14].

In this manuscript, MgO doped zirconia mullite were prepared following plasma fusion, plasma sintering and conventional sintering techniques. A complete conversion of zirconia mullite from sillimanite, zircon and alumina mixture is observed in plasma-fused composites whereas a small percentage of sillimanite and zircon is observed in plasma and conventionally sintered specimen. This evidence represents that the temperature provided by plasma and conventional sintering is not sufficient for the 100% dissociation of sillimanite and zircon.

2. Experimental detail

The MgO doped zirconia mullite (MgO–MUZ) composites were prepared using the heating sources like the plasma reactor and the high temperature programmable furnace from the raw materials like Indian coastal sillimanite, zircon beach sand, alumina and MgO powder. The major raw materials sillimanite and zircon were obtained from Indian rare-earth limited (IREL), Chhatrapur, India. The SEM pictures of sillimanite and zircon grains are given in Fig. 1. Sillimanite grains are of euhedral shape mostly occurring in acicular and rectangular form (Fig. 1a) whereas zircon grains are of ovoidal and cylindrical in shape (Fig. 1b). The average grain size of sillimanite minerals are in the order of 200–300 μm whereas the average grain size of zircon is in the order of 400–500 μm. For proper mixing and to reduce the particle sizes to micron, all these grains are grinded by using a swing mill grinder (make: HERZOG Maschinenfabrik).

Sillimanite, alumina and zircon were taken in the wt. ratio of 47:38:15 (which corresponds to SiO_2, Al_2O_3 and ZrO_2 weight ratio of 23:67:10), to which 16 mole% of MgO is added with respect to the ZrO_2 content for the synthesis of MgO–MUZ composites. The mixture is well mixed using a Retsch PM 100 ball mill grinder to reduce the particle sizes to less than a micron. The SEM picture obtained for the above compositional mixture is given in Fig. 2. The average particle sizes are of 1 μm.

The synthesis techniques adopted for the synthesis of MgO–MUZ composites are those consisting mainly of the plasma fused, plasma sintering and conventional sintering processes. The detailed descriptions of the melting and sintering techniques are presented below.

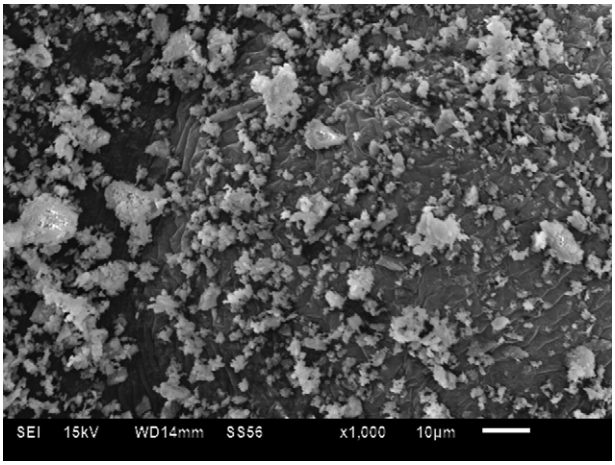

Fig. 2. Scanning electron microscopy picture of sillimanite, zircon, alumina and MgO mixture after grinding in a mixture grinder.

An indigenously developed 50 kW thermal plasma reactor was used for plasma fused and plasma sintering techniques. Argon was used as the plasmagen gas in the reactor with a constant flow rate (∼1 l/min). The schematic picture of the thermal plasma reactor and the details of the reactor are discussed briefly elsewhere [15,16]. A water-cooled stainless steel double-walled cylindrical chamber (outer) was fixed with suitable thermal insulation like bubble alumina for the confinement of plasma heating. High-pressure cold water was allowed to flow throughout the external body of the reactor. Necessary rack-pinion arrangements were made for fine adjustment of the electrode distance to obtain the required arc length. Plasma forming gas (argon) flow into the electrode space was provided through a narrow hole of the upper electrode (cathode). The mixed powders in the required ratio were fed to the plasma reactor and were directly exposed to plasma for 5 min with a plasma power of 15 kW (300 A-DC current and 50 V-DC voltages) for the synthesis of fused MgO–MUZ. The synthesis of fused MgO–MUZ takes place in the liquid state of alumina, silica and zirconia [15,16] in the DC extended thermal plasma reactor. It is expected to enhance the

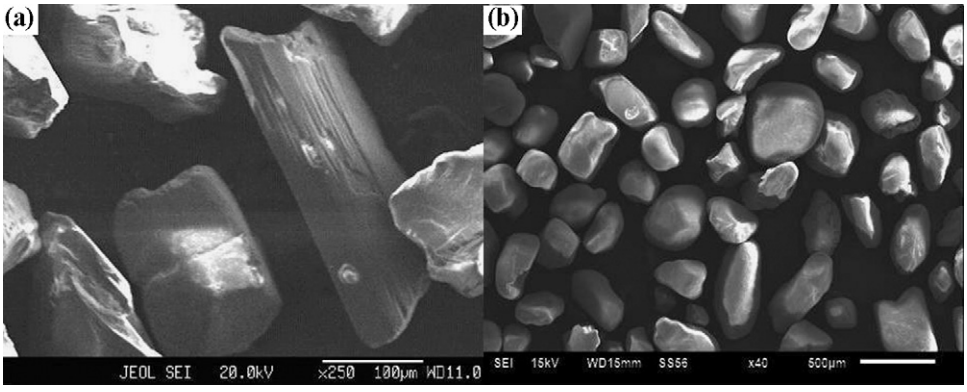

Fig. 1. Scanning electron microscopy picture of (a) sillimanite and (b) zircon.

reaction kinetics which in turn reduces the processing time to 5 min.

Cylindrical pellets of the material with the above-mentioned compositional ratio having 5 g weight and 10 mm diameter were prepared using 0.5 mole% polyvinyl alcohol (PVA) as a binder under a pressure of about 8 T/cm^2 for the synthesis of plasma and conventionally sintered samples. The pellets thus prepared were heated at 700 °C for 2 h to get the pre-handling strength, to remove the PVA binder and other volatiles (if present) and then used for sintering by thermal plasma reactor using a special type of graphite sample holder designed by us. The schematic picture of the graphite sample holder is presented elsewhere [16]. The sample holder was placed coaxially (vertical direction) between the electrodes of the plasma reactor. Heavyweight graphite base was placed near to the sample holder to hold the temperature of the arching zone of the plasma reactor. Rack and pinion arrangements were attached to the reactor vessel, in order to control accurately the plasma arc length and plasma sustainability under particular plasma power. The calcined pellet of MgO–MUZ composites were placed symmetrically inside the sample holder and fixed coaxially to the lower electrode. The graphite sample holder was placed coaxially along the plasma arc length. This technique of using DC extended arc thermal plasma for sintering the MgO–MUZ is known as the rapid sintering technique. The samples in this case were heated by plasma for 15 min (instead of 5 min as in plasma fused case) with a plasma power of 15 kW (300 A-DC current and 50 V-DC voltages), as the samples were not directly exposed to plasma, being placed in the graphite sample holders. The approximate temperature reached during the plasma sintering is around 1500–1600 °C. This type of rapid sintering technique prohibits the grain growth. The parameters used for plasma fused and plasma sintering techniques were optimized after performing several experiments.

For the synthesis of MgO–MUZ by conventional sintering technique, the pellets prepared following the above procedure were sintered at 1450 °C for 5 h at a heating rate of 50 °C/h and cooling rate of 300 °C/h using programmable high temperature furnace (Therlek Make). Such type of conventional sintering schedule provides longer time to the particles for proper diffusions and reactions. The detail parameter of sintering schedule for plasma fusion, plasma sintering and conventional sintering are listed in Table 1.

The bulk density and porosity of the samples were measured (using the Archimedes' principle) according to ASTM specification D792-00. Hardness of the composites was measured according to ASTM Standard E384 using LECO hardness tester (LM247AT) by Vickers microindentation hardness testing method with an applied load of 100 gf for 13 s on the mullite phase. The structural characterizations and identification of different mineral species were carried out by X-ray diffraction (XRD) technique using Cu Kα radiation. The unit cell lattice parameter and unit cell volume were calculated on the basis of experimental results using WinCell XRD software through Rietveld Refinement. Electron micrographs analysis was carried out using scanning electron microscopy (SEM). Diffuse reflective spectroscopy (DRS) studies have been carried out to determine the band gap of MgO–MUZ using UV–vis spectrophotometer (model: Varian Cary 100).

3. Results and discussions

Fig. 3 shows the XRD pattern of sillimanite, zircon and all the MgO–MUZ samples. The XRD pattern shown in Fig. 3a having all the reflection peaks correspond to sillimanite which is well agreement with the JCPDS # 89-1483. A small percentage of iron is present in the specimen which cannot be detected due to the XRD instrumental limitation. Similarly, the XRD pattern obtained for zircon (Fig. 3b) shows all the major reflection peaks and is matched with the JCPDS # 83-1383. The small percentage of other impurities present in the specimen cannot be detected due to the XRD instrument limitations. These two patterns are taken as the standard to determine phase transformation from sillimanite and zircon to mullite and zirconia after the heat treatment done by plasma reactor and conventional heating furnace. Fig. 3c–e shows the XRD patterns of plasma fused, plasma sintered and conventionally sintered MgO–MUZ.

The presence of mullite and zirconia is clearly seen in the XRD spectrum of plasma fused samples (Fig. 3c). Presence of monoclinic, tetragonal and cubic zirconia is observed. During the synthesis of plasma-fused specimen, the reactor attained an approximate temperature of 2100 °C. The sillimanite and zircon taken for the synthesis of MgO–MUZ dissociates at this temperature and a homogeneous reaction is occurred in between alumina and silica; forms the mullite phase. Hence, no phases related to zircon and sillimanite is found in the plasma-fused composites. As the temperature is so high, the monoclinic phase of zirconia is converted to the tetragonal and cubic phase. Hence, a mixture of monoclinic, tetragonal and cubic phase of zirconia is obtained in the XRD pattern. In thermal plasma reactor, two kinds of cooling phenomena are observed. One is due to furnace cooling and the other one is due

Table 1
Various process parameters used in plasma fused, plasma sintered and conventional sintered MgO–MUZ.

Synthesis methods	Name of the composites	Power used in plasma reactor	Time of plasma exposed
Plasma fused	MgO–MUZ	15 kW	5 min
Plasma sintered	MgO–MUZ	15 kW	20 min

Synthesis methods	Name of the composites	Temperature set in high temperature furnace	Dwell time
Conventionally sintered	MgO–MUZ	1450 °C	5 h

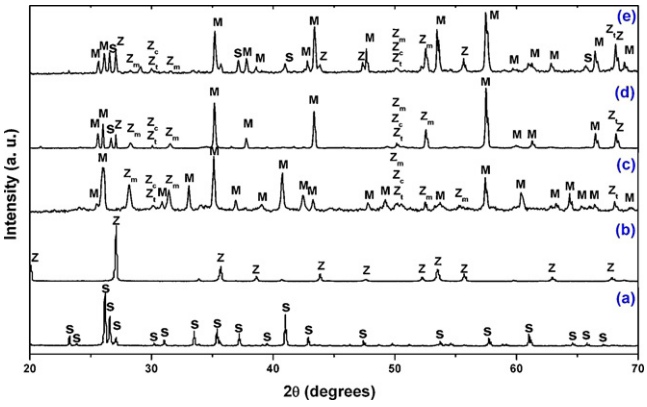

Fig. 3. XRD pattern of (a) sillimanite; (b) zircon; (c) plasma fused MgO–MUZ; (d) plasma sintered MgO–MUZ; and (e) conventionally sintered MgO–MUZ.

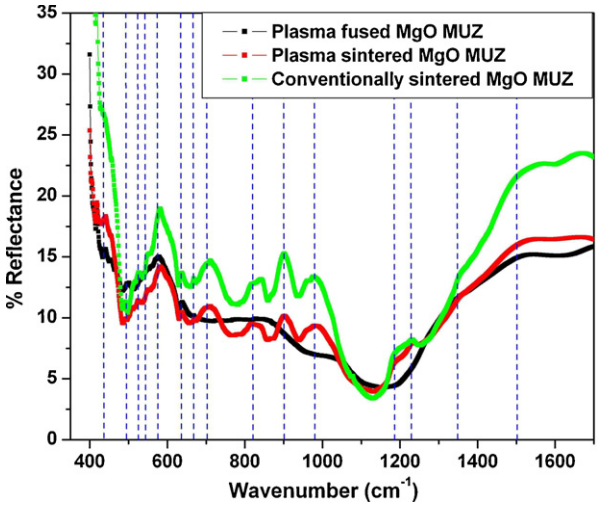

Fig. 4. FTIR spectra of MgO–MUZ composites.

to the sharp temperature thermal gradient owing to plasma. The rapid cooling of the system stabilizes the cubic phase of zirconia without going to reverse transformation to monoclinic phase, whereas the slow cooling provides enough time to regain the monoclinic phase of zirconia. This is the reason why monoclinic phase of zirconia is predominant over the tetragonal and cubic zirconia phase.

In plasma and conventional sintering process, the total percentage of sillimanite and zircon is not dissociated completely for the formation of zirconia/mullite aggregates for which zircon and sillimanite peaks are seen in the XRD patterns (Fig. 3d and e). In plasma sintering process, the temperature is not so enough (≈1500–1600 °C) and also the heat is confined in the graphite crucible for which, it does not able to provide sufficient temperature to dissociate sillimanite and zircon completely and to stabilize the cubic phase of zirconia. Similar type of phenomenon is observed in the conventionally sintered composites. Hence secondary phases of zircon and sillimanite have been observed in the XRD patterns. Even the temperature in the plasma sintering and conventional sintering are lower than the transformation temperature of monoclinic phase of zirconia to cubic phase of zirconia, MgO favors this transformation and also stabilize the cubic zirconia phase. The unit cell lattice parameter of mullite estimated for all the MgO–MUZ composites are listed in Table 2.

The FTIR spectra of all the composites are shown in Fig. 4. The reflectance peaks correspond to 544 cm^{-1}, 824 cm^{-1}, 979 cm^{-1} and 1504 cm^{-1} are attributed to the signature of Si–O–Al (mullite) [17]. These peaks are present in all the composites. The vibrational modes of silica are found in the spectra at 669 cm^{-1}, 702 cm^{-1}, 903 cm^{-1} and 1187 cm^{-1} which are coming from the undissociated sillimanite and zircon. These peaks are absent in plasma fused MgO–MUZ composites. It means that the total amount of sillimanite and zircon is completely dissociated and there is complete formation of zirconia/mullite aggregates in plasma-fused composites. This fact is completely matched with the XRD pattern. The peaks presented at 443 cm^{-1}, 494 cm^{-1}, 526 cm^{-1} and 573 cm^{-1} are attributed to the Zr–O bonds [18,19].

The SEM picture of plasma-fused specimen is shown in Fig. 5. It shows hexagonal and tetragonal platelet structure. These platelets are elongated in various directions. The surfaces of the platelets are representing the mullite phase (Fig. 5a) whereas zirconia is embedded in the grain boundary region. A small percentage of zirconia is found in the intragrain region of mullite. Tree like clusters of zirconia is found on the mullite surface (Fig. 5b). There are a lot of micro-cracks observed on the mullite surface (Fig. 5b). In plasma-fused specimen, zirconia is present in the alumina and silica melt. So while sudden switching off the plasma arc, the zirconia forms a cluster in the intragrain region of the mullite melt and gives rise to the dendrite structure.

The plasma-sintered micrograph shows a ladder like structure and a complete cross-linked in between the mullite grains (Fig. 6a). Some surfaces show the presence of small grains interconnected to each other with a significant number of microcracks and voids (dark colored spot). The inter-granular spacing and percentage of porosity is less in comparison to the plasma fused and conventionally sintered composites. The surface morphology of conventionally sintered composites

Table 2
Unit cell lattice parameter and unit cell volume of mullite in plasma fused (PF), plasma sintered (PS) and conventionally sintered (CS) MgO–MUZ.

Unit cell lattice parameter/volume of mullite	PF MgO–MUZ	PS MgO–MUZ	CS MgO–MUZ	Remark (compared with the reported mulllite; JCPDS #150776)
a (Å)	7.507	7.499	7.517	7.545
b (Å)	7.784	7.775	7.708	7.689
c (Å)	2.892	2.880	2.876	2.884
V ($Å^3$)	168.99	167.95	166.64	167.35

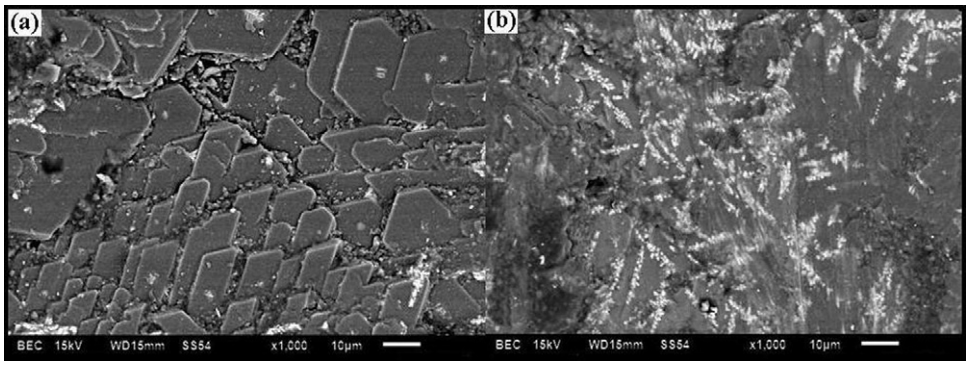

Fig. 5. Scanning electron micrographs of plasma fused MgO–MUZ composites (a) showing tetrahedral platelet and (b) dendritic zirconia.

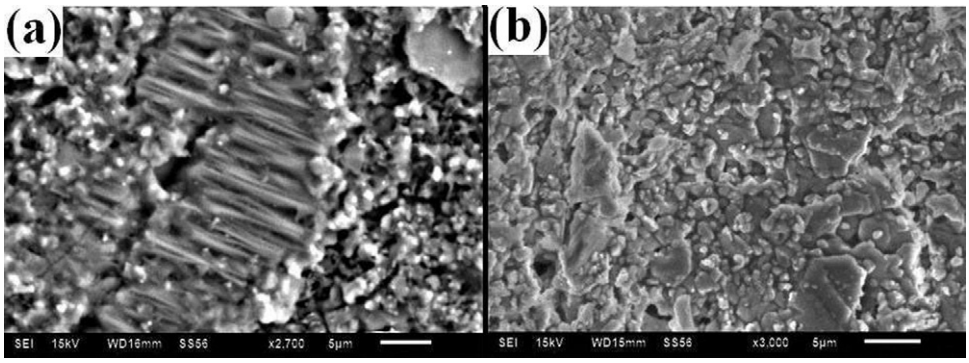

Fig. 6. Scanning electron micrographs of (a) plasma sintered MgO–MUZ composites and (b) conventionally sintered MgO–MUZ composites.

clearly indicates the presence of small and big grains close packed to each other (Fig. 6b). From the SEM analysis for all the composites, it is realized that the additive MgO acts as sintering aid for the formation of well-interconnected and cross-linked grains. The bulk densities of the materials are depended on the microstructure of the composites.

The bulk density of MgO–MUZ composites prepared by plasma fusion, plasma sintering and conventional sintering technique was measured by Archimedes' technique. The bulk density of plasma fused, plasma sintered and conventionally sintered specimen are 2.71 g/cm^3, 3.25 g/cm^3 and 3.03 g/cm^3. The percentage of porosity (2.99) is more in plasma-fused specimen which reduces the bulk density whereas the percentage of porosity is only 1.55 in plasma sintered specimen. The bulk density of plasma-sintered specimen is approximately equal to the theoretical value of mullite (3.31 g/cm^3). This fact is well supported by the SEM studies done for all the composites.

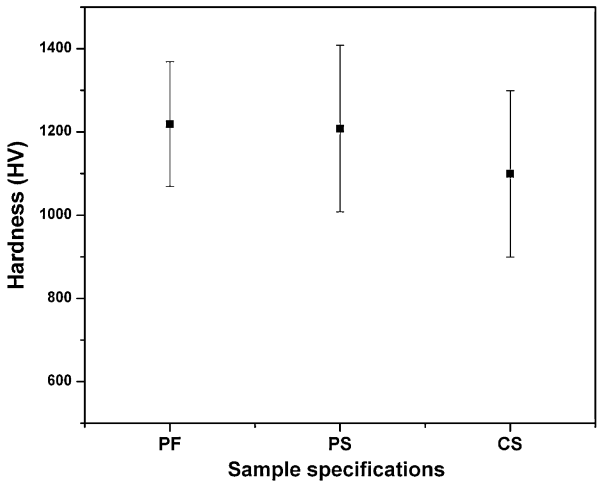

Fig. 7. The curve represents the hardness vs. sample specifications (The abbreviations PF, PS and CS indicate Plasma fusion, plasma sintered and conventionally sintered MgO-MUZ composites respectively).

Fig. 7 shows the hardness vs. sample specifications. There is not much variation in the hardness in all the synthesized mullite/zirconia aggregates. In general, the microstructure is mostly responsible for the variation of hardness in the entire specimen. As described in electron micrograph, mullite platelet and dendritic zirconia structure with no micro-cracks are found in the microstructure of plasma-fused composites whereas the well-connected ladder like structure are observed in plasma sintered composites. However the well compaction of big grains and small grain gives an appreciable hardness to the conventionally sintered composites. Here MgO plays an important role in the formation of well connected and close packed structure with a small number of voids. Hence the variation in hardness is not observed in all the composites even the variation in various components like mullite, zirconia, sillimanite and zircon have been observed in XRD and FTIR patterns.

The optical band gap of MgO–MUZ composites were studied by UV–vis spectroscopy using reflectance mode of operation and are shown in Fig. 8. The optical band gap of

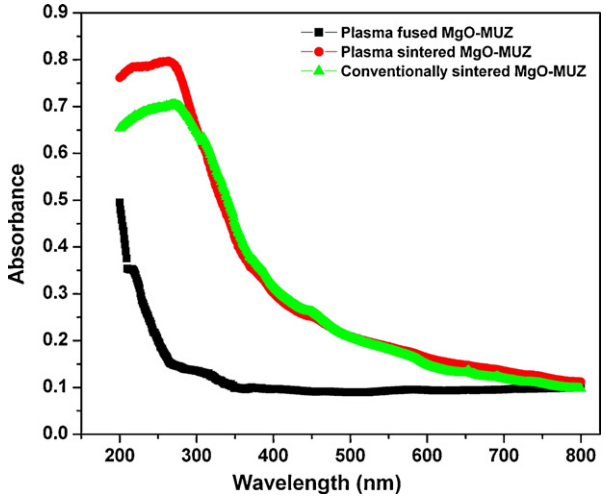

Fig. 8. Diffuse reflectance spectra of MgO–MUZ composites.

plasma fused, plasma sintered and conventionally sintered MgO–MUZ composites as determined from the discontinuity of the $d\{\ln(\alpha h\nu)\}/d(h\nu)$ curve (where "α" is the optical absorption coefficient and $h\nu$ is the photon energy) [20] (not shown) are 4.22 eV, 2.84 eV and 2.74 eV respectively. There is not much variation in the optical band gap in plasma sintered and conventionally sintered MgO–MUZ composites. However, the higher band gap observed in plasma fused MgO–MUZ is due to the complete dissociation of sillimanite and zircon and conversion of 100% mullite phase and zirconia.

4. Conclusions

In conclusion, complete dissociation of sillimanite and zircon has been occurred for the conversion of zirconia/mullite aggregates in plasma fused MgO–MUZ composites within the 5 min of plasma arching. The additive MgO in MUZ not only stabilizes the cubic zirconia phase but also creates the cross-linking between the mullite grains. Uniform arrangement of mullite platelets and dendritic structure of zirconia has been observed in the surface of plasma fused MgO–MUZ composites whereas ladder like structure with complete interconnected mullite grains has been observed for plasma sintered composites. Appreciable hardness and higher optical band gap have been observed for plasma fused MgO–MUZ composites. The total sillimanite and zircon mixtures have been utilized for the complete conversion of mullite and zirconia composites in plasma fusion whereas the complete conversion of sillimanite and zircon has not observed in plasma sintered and conventionally sintered composites.

Acknowledgement

Authors are very much thankful to Director, IMMT, Bhubaneswar for providing research support to carry out this research.

References

[1] H. Schneider, S. Komarneni (Eds.), Mullite, WILEY-VCH Verlag GmbH & Co. KGaA, Weinheim, 2005.
[2] P.M. Suoto, R.R. Menezes, R.H.G.A. Kiminami, Effect of Y_2O_3 additive on conventional and microwave sintering of mullite, Ceramics International 37 (2011) 241–248.
[3] M.N. Ibarra Castro, J.M. Almanza Robles, D.A. Cortes Hernandez, J.C. Escobedo Bocardo, J. Torres, Development of mullite/zirconia composites from a mixture of aluminum dross and zircon, Ceramics International 35 (2009) 921–924.
[4] S. Yugeswaran, V. Selvarajan, P. Dhanasekarana, L. Lusvarghi, Transferred arc plasma processing of mullite–zirconia composite from natural bauxite and zircon sand, Vacuum 83 (2008) 353–359.
[5] B.-Y. Ma, Y. Li, S.-G Cui, Y.-C Zhai, Preparation and sintering properties of zirconia–mullite–corundum composites using fly ash and zircon, Transactions of Nonferrous Metals Society of China 20 (2010) 2331–2335.
[6] N.M. Rendtorff, L.B. Garrido, E.F. Aglietti, Mullite–zirconia–zircon composites: properties and thermal shock resistance, Ceramics International 35 (2009) 779–786.
[7] N.M. Rendtorff, L.B. Garrido, E.F. Agiletti, Zirconia toughening of mullite–zirconia–zircon composites obtained by direct sintering, Ceramics International 36 (2010) 781–788.
[8] A.A. Sharif, M.L. Mecatney, Superplasticity in cubic yttria stabilized zirconia with 10 wt.% alumina, Journal of European Ceramic Society 24 (2004) 2041–2047.
[9] S. Tekeli, M. Erdogan, B. Aktas, Influence of α-Al_2O_3 addition on sintering and grain growth behavior of 8 mole% Y_2O_3-stabilized cubic zirconia (c-ZrO_2), Ceramics International 30 (2004) 2203–2209.
[10] X.-H Jin, L. Gao, Y.-M Kan, Y.-R Chen, Q.-M. Yuan, Influence of Nb_2O_5 on the mechanical performances and toughening mechanism of ZrO_2 in ZTM–Al_2O_3, Journal of Inorganic Materials 15 (2000) 1009–1014.
[11] T. Ebadzadeh, E. Ghasemi, Effect of TiO_2 addition on the stability of t-ZrO_2 in mullite–ZrO_2 composites prepared from various starting materials, Ceramics International 28 (2002) 447–450.
[12] L.B. Garrido, E.F. Aglietti, Reaction-sintered mullite–zirconia composites by colloidal processing of alumina–zircon–CeO_2 mixtures, Materials Science Engineering A 369 (2004) 250–257.
[13] S. Maitra, S. Pal, S. Nath, A. Pandey, R. Lodha, Role of MgO and Cr_2O_3 additives on the properties of zirconia–mullite composites, Ceramics International 28 (2002) 819–826.
[14] P. Descamp, S. Sagakuchi, M. Portemon, F. Cambier, High temperature characteristics of reaction-sintered zirconia–mullite composites, Journal of American Ceramic Society 74 (1991) 2476–2481.
[15] S. Prusty, D.K. Mishra, B.K. Mohapatra, S.K. Singh, Correlation between properties of zirconia mullite and Y_2O_3 stabilized zirconia mullite derived by various processing techniques, Advances in Applied Ceramics 110 (2011) 360–366.
[16] D.K. Mishra, S. Prusty, B.K. Mohapatra, S.K. Singh, A comparative study of CaO–MUZ elaboration by plasma melting and sintering technique, Materials and Manufacturing Processes, (2011), doi:10.1080/10426914.2011.577870, in press.
[17] V. Gomez-Serrano, M.C. Fernandez-Gonzalez, M.L. Rojas-Cervantes, M.F. Alexandre-Franco, A. Macias-Garcia, Carbonization and demineralization of coals: A study by means of FT-IR spectroscopy, Bulletin of Materials Science 26 (2003) 721–732.
[18] M. Maczka, E.T.G. Lutz, H.J. Verbeekc, K. Oskamd, A. Meijerinkd, J. Hanuza, M. Stuivingac, Spectroscopic studies of dynamically compacted monoclinic ZrO_2, Journal of Physics and Chemistry of Solids 60 (1999) 1909–1914.
[19] G. Duan, C. Zhang, A. Li, X. Yang, L. Lu, X. Wang, Preparation and characterization of mesoporous zirconia made by using a poly (methyl methacrylate) template, Nanoscale Research Letter 3 (2008) 118–122.
[20] D. Bhattacharya, S. Choudhary, A.K. Pal, Bandgap and optical transitions in thin films from reflectance measurements, Vacuum 43 (1992) 313–316.